Frequency Control in Isolated/Islanded Microgrids Through Voltage Regulation

Mostafa Farrokhabadi, *Student Member, IEEE,* Claudio Cañizares, *Fellow, IEEE* and Kankar Bhattacharya, *Senior Member, IEEE*

***Abstract*—This paper presents a frequency control mechanism for an isolated/islanded microgrid through voltage regulation. The proposed scheme makes use of the load voltage sensitivity to operating voltages and can be easily adopted for various types of isolated microgrids. The proposed controller offers various advantages, such as allowing the integration of significant levels of intermittent renewable resources in isolated/islanded microgrids without the need for large energy storage systems, providing fast and smooth frequency regulation with no steady-state error, regardless of the generator control mechanism. The controller requires no extra communication infrastructure and only local voltage and frequency is used as feedback. The performance of the controller is evaluated and validated through various simulation studies in the PSCAD/EMTDC software environment based on a realistic microgrid test system, using small-perturbation stability analysis to demonstrate the positive effect of the proposed controller in system damping.**

***Index Terms*—Isolated Microgrid, Distributed Energy Resources (DER), Frequency Control, Voltage Regulation.**

I. Introduction

Isolated microgrids have been shown to be a reliable and efficient solution to provide energy for remote communities [1]. In addition, with IEEE 1547 standard permitting the islanded operation of distribution networks [2], isolated/islanded microgrids will become more prevalent, improving the reliability of electricity supply and allowing better integration of renewable energy sources [3]. Similar to large interconnected systems, these microgrids should meet certain required reliability and adequacy standards, which demand all controllable units to be actively involved in maintaining the system voltage and frequency within acceptable ranges. However, due to the low system inertia and fast changes in the output power of wind and solar power sources, the microgirds frequency can experience large excursions and thus easily deviate from nominal operating conditions [4], even when there is sufficient frequency control reserves; hence, it is challenging to control the frequency around the nominal operating point [5].

Several papers discuss control techniques for operation of microgrids [6]–[8]. In [9], a control strategy is proposed to emulate the conventional droop control mechanism, providing the ability to distribute the total demand amongst distributed generator (DG) units using local feedback signals, without the need for communications. This makes the droop mechanism one of the most appropriate controls for isolated microgrids, where access to communication infrastructure is limited. However, the stability of the microgrid with droop controls examined in [10] demonstrates that although increasing the droop gains improves the power sharing, it adversely affects the overall system stability.

In view of the limitations of droop control, numerous strategies have been proposed for frequency control and power sharing in isolated/islanded microgrids, mainly to improve the transient response of the system by introducing a supplementary control loop [11]–[13]. All these methods are built on top of the conventional drooping mechanism, which results in steady-state frequency error. To overcome this drawback, a load-angle droop is introduced to replace the traditional frequency droop in [14], [15]. However, it is shown in [15] that load sharing and system stability margin deteriorates under this paradigm. Furthermore, all the methods in [11]-[15] rely on microgrids with dispatchable, electronically interfaced distributed energy resources (DERs), while the majority of isolated micorgrids, specially in remote communities, rely on synchronous machines with diesel engines [16].

Generally, and in addition to previously highlighted shortcomings, droop controllers may exhibit poor frequency regulation due to rapid changes in the output power of the DGs [17]. Thus, there is a need for additional frequency controls, especially in islanded microgrids with high penetration of renewable energy sources. A long-established strategy is dynamic demand control (DDC), i.e. reducing the consumption of the loads by directly turning them off or changing their operating voltage [18]. For example, the Pacific Northwest National Laboratory (PNNL) has developed a load controller that detects major deviations in the grid frequency and turns off appliances accordingly [19]. Various other centralized and decentralized DDC approaches have been reported in the literature [20]. However, these techniques are not viable for isolated microgrids, especially those in remote communities, as DDC requires significant communication infrastructure and controllers to be installed at each individual appliance.

In [21], a supplementary loop is introduced in the control system of variable-speed wind turbines to extract power from the rotating mass of the turbines. This strategy emulates the response of a conventional synchronous generator, and adds virtual inertia to the system, but this is limited by the speed and power rating of the turbines; furthermore, the recovery period of the turbine is an issue, as highlighted in [22]. In addition to these control strategies, hardware solutions are proposed

This work was supported by NSERC Smart Microgrid Network (NSMG-Net), Hydro One Inc., ABB Corporation Research Center USA and IBM Canada Inc..

The authors are with the Department of Electrical and Computer Engineering, University of Waterloo, Waterloo, ON N2L 3G1, Canada (e-mail: m5farrok@uwaterloo.ca; ccanizares@uwaterloo.ca; kankar@ece.uwaterloo.ca).

to tackle the problem of low inertia and frequency control in microgrids. Thus, in [23], the use of highly flexible conventional units such as synchronous generators is suggested, which provide extra rotating mass, and hence extra inertia for the system; however, this is a costly solution, and requires investing in new generation units for the system, with power losses and maintenance costs being also major concerns.

Energy storage systems (ESS) are a practical and viable option for isolated/islanded microgrids with high penetration of renewable energy sources, allowing for proper frequency and voltage control. Thus, in [22], it is demonstrated that fast acting ESS considerably reduces the impact of wind and solar generation on isolated microgrid inertia. However, ESS are expensive, and require special maintenance and slightly larger inverters, with limited useful life-time.

In view of all the aforementioned issues with regard to proper frequency control in isolated/islanded microgrids, this paper proposes a state-of-the-art frequency control approach that is built on top of existing decentralized frequency control methods, providing a virtual reserve for the system. The controller utilizes the load power sensitivity to operating voltage to maintain the system active power balance, thus properly controlling frequency. Specifically, the proposed controller offers the following advantages:

- It reduces the dependency of isolated microgrids on ESS to regulate the active power mismatch, and hence frequency.
- It facilitates nominal steady-state frequency operation without the need for additional controls.
- It works with any type of DG, i.e. converter and machine based, with voltage control capability, maintaining voltages within acceptable ranges.
- Only local feedback signals are required, i.e. there is no need for communications.
- Its response is fast, and thus especially adequate for rapidly varying wind and solar power sources, preventing frequency excursions.
- It improves the system damping.

The rest of the paper is organized as follows: Section II describes the operating principles of voltage and frequency control in power systems. In Section III, the proposed voltage frequency control strategy is explained along with its underlying concepts. Section IV demonstrates the effectiveness of the proposed controller through eigenvalue studies and various time domain simulations performed in the PSCAD/EMTDC platform in a realistic test microgrid; it also discusses various aspects that affect the performance of the proposed controller. Finally, Section V presents the main contributions and conclusions of the presented work.

II. Principles of Frequency and Voltage Control

A. Synchronous Machine [24]

In power systems with rotating components such as synchronous generators and motors, any mismatch between active power generation and demand results in a frequency deviation, which is instantaneously compensated by an alteration in kinetic energy of the rotating mass in the system. For small disturbances, with frequency deviation Δf, the rate of change of frequency (ROCOF) can be calculated as follows:

$$\frac{d\Delta f(t)}{dt} = f_0 \frac{P_m(t) - P_e(t)}{2W_K} = f_0 \frac{\Delta P_{pu}(t)}{2H} = \frac{\Delta P_{pu}(t)}{M} \quad (1)$$

where P_m and P_e are mechanical and electrical power respectively; W_k is the total kinetic energy stored in the rotating mass of the system; and $H = W_K/S_{base}$, and $M = 2H/f_0$ are the system inertia constants.

If the generation reserve is sufficient, then the primary frequency control restores the power equilibrium to make ROCOF zero. Otherwise, automatic load shedding procedures are required to disconnect a portion of the active load to restore the active power balance. In systems with a single generator, it is possible to maintain the steady-state nominal frequency by compensating change in load power ΔP_D, and increasing the active power generation until the system reaches the nominal frequency. However, such a mechanism is not practical in an interconnected system with more than one generator, because each generator will oppose the other, trying to compensate for any change in the power mismatch alone. In such a system, the frequency is allowed to change according to the active power output and is used as a feedback signal to determine the appropriate load sharing among the generators; this is referred to as droop control [24]. In this case, the system will have a steady-state error in the frequency.

The slope of the power-frequency relationship is a unique characteristic of each generator and is referred to as the speed regulation or droop (R), and is defined as follows:

$$R\% = \frac{\omega_{NL} - \omega_{FL}}{\omega_0} \times 100 \quad (2)$$

where ω_{NL} is the no-load steady-state speed, ω_{FL} is the full-load steady-state speed, and ω_0 is the rated speed. Under the frequency droop paradigm, the generator with higher R participates less in compensating for load perturbations in the system, since:

$$\Delta P_g = \Delta P_{ref} - \frac{1}{R}\Delta\omega \quad (3)$$

where ΔP_G is the change in the active power output of a generator.

Voltage control in synchronous machines is carried out by the excitation system, which supplies dc current to the synchronous machine field winding, and adjusts the current to maintain the generator terminal voltage. Several different excitation systems have been developed [25], with all sharing the same operating principle as the basic regulator shown in Fig. 1 [26], where the generator terminal voltage V_t is compared with the voltage reference set-point V_{ref} to obtain the voltage error signal ΔV. The error signal is passed through a regulator where τ_r represents the voltage regulator time delay. Afterwards, the output of the voltage regulator V_r is applied to the exciter, where τ_e represents the exciter time constant. Finally, the output of the exciter E_{fd}, determines the generator field winding voltage, which subsequently adjusts the generator terminal voltage. The compensator block shown in Fig. 1 improves the excitation system dynamic response by reducing the excessive overshoot.

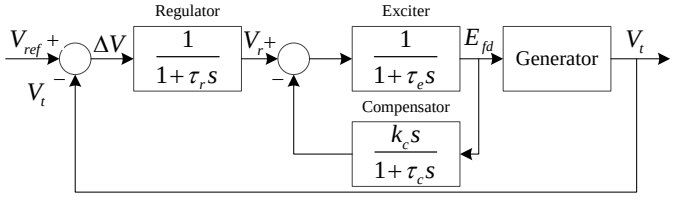

Fig. 1. Basic generator excitation system [26].

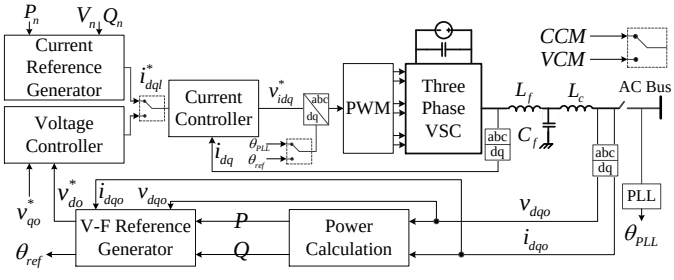

Fig. 2. Control structure of an electronically interfaced DER or ESS.

B. Converter-based DER and ESS

The general schematic of a DER connected to a system via a bidirectional voltage source converter (VSC) is shown in Fig. 2. The VSC is connected via an LC filter, along with a coupling inductor L_c, and has two different control modes, i.e. the voltage control mode (VCM) and the current control mode (CCM). CCM is adopted in this paper as the control strategy for the inverters.

Under the CCM paradigm, the output active power, and either the reactive power or voltage reference set-points are fed to a current reference generator to obtain the d-axis and q-axis reference current set-points I_{ld}^* and I_{lq}^*, respectively, through PI controllers, as follows:

$$\frac{d\upsilon}{dt} = V_n - V_o \quad \frac{d\Psi}{dt} = P_n - P \tag{4}$$

$$I_{ld}^* = K_{p1}\left(P_n - P\right) + K_{i1}\Psi \tag{5}$$

$$I_{lq}^* = K_{p2}\left(V_n - V_o\right) + K_{i2}\upsilon \tag{6}$$

where υ and ψ are output signals of the integrators, and K_p and K_i are the P gain and I gain, respectively.

III. Proposed Voltage-based Frequency Controller (VFC)

A. Loads Voltage Dependency

The loads in a power system are typically modelled by the following equation [24]:

$$P = P_0\left(\frac{V}{V_0}\right)^{n_p} \tag{7}$$

which can be viewed equivalently as a ZIP load:

$$P = P_0\left[Z_p\left(\frac{V}{V_0}\right)^2 + I_p\left(\frac{V}{V_0}\right) + P_p\right] \tag{8}$$

$$n_p \approx \frac{2\times Z_p + 1\times I_p + 0\times P_p}{Z_P + I_p + P_p} \tag{9}$$

and similarly for:

$$Q = Q_0\left(\frac{V}{V_0}\right)^{n_q} \tag{10}$$

$$Q = Q_0\left[Z_q\left(\frac{V}{V_0}\right)^2 + I_q\left(\frac{V}{V_0}\right) + P_q\right] \tag{11}$$

$$n_q \approx \frac{2\times Z_q + 1\times I_q + 0\times P_q}{Z_q + I_q + P_q} \tag{12}$$

where P is the active power demand; Q is the reactive power demand; P_0 is the rated active power, and Q_0 is the rated reactive power at nominal operating voltage V_0; and n_p and n_q are voltage indexes for the active power and reactive power respectively; Z_p, I_p and P_p are the constant impedance, constant current and constant power coefficients. As it can be seen from (7), the active power demand sensitivity to the operating voltage ($\partial P/\partial V$) is determined by n_p; thus as n_p increases, the sensitivity of power consumption with respect to operating voltage also increases. In [27], a comprehensive study is carried out to model residential loads that shows an average n_p for existing residential load models in the range of 1.1 to 1.7. This value is expected to be even higher in isolated microgrids, where the majority of the power is consumed by households for heating and lightning purposes (resistive loads).

Throughout this paper, two different n_p are assumed, $n_p = 1.5$ ($Z_p = 0.6$, $I_p = 0.3$, $P_p = 0.1$) and $n_p = 1.2$ ($Z_p = 0.3$, $I_p = 0.6$, $P_p = 0.1$). For a system with $n_p = 1.5$, a change in the operating voltage ΔV will result in an active power demand change ΔP_D as follows:

$$\Delta P_D = \left((V + \Delta V)^{1.5} - V^{1.5}\right)\frac{P_0}{V_0^{1.5}} \tag{13}$$

Assuming that V and V_0 are both 1 pu, i.e. the loads were operating at their nominal operating voltage prior to change, (13) can be re-written as follows:

$$\Delta P_D = \left((1 + \Delta V)^{1.5} - 1\right)P_0 \tag{14}$$

From (14), it can be estimated that in a system with $n_p = 1.5$, a 5% decrease in the operating voltage will reduce the active power demand by around 7.6%. In other words, a relatively slight drop in the operating voltage results in a comparable demand reduction. Hence, this strategy is utilized in this paper to provide a virtual reserve capacity in the system. This virtual reserve capacity, provisioned from the VFC proposed in this paper, should have an instantaneous effect on the system demand and would decrease the need for investing in ESS, as demonstrated in Section IV.

B. Proposed Voltage-based Frequency Controller (VFC)

Figure 3 shows the proposed VFC for an isolated microgrid. The input signal to the controller is the system frequency deviation from the nominal set-point Δf. The frequency error is passed through a PI controller to ensure that the steady-state error is zero, and the gain K_{VFC} determines the damping factor provided by the VFC. The signal is passed through a lead-lag block to compensate for the phase difference between the voltage regulator input and output; to obtain the best

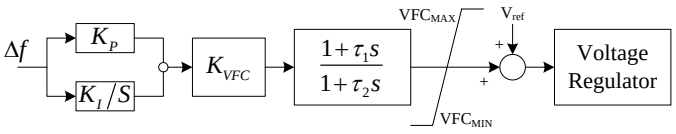

Fig. 3. The proposed VFC for a system voltage regulator, such as the one for a synchronous machine.

response, more than one lead-lag block may be used in practice. The limits VFC_{max} and VFC_{min} constrain the output signal to ensure that the voltage remains within a desired range. The output signal of the VFC is then added to the reference set-point signal of the voltage regulator V_{ref}. The ideal transfer function of the VFC is as follows:

$$G_{VFC}(s) = K_{VFC}\frac{1+\alpha s+\beta s^2}{\tau_i s+\gamma s^2} \tag{15}$$

$$\alpha = (K_P+1)\tau_i+\tau_2 \quad \beta = K_P\tau_i\tau_2+\tau_i\tau_1 \quad \gamma = \tau_i\tau_2 \tag{16}$$

where $\tau_i = \frac{1}{K_I}$, τ_1 and τ_2 are the integrator and lead-lag block time constants, and K_P is the proportional gain.

Care should be taken to tune the controller so as to ensure the overall system stability. In addition, the controller gain K_{VFC} should properly address the relation between the system operating frequency and the voltage. For this paper, the VFC parameters are given in Section IV, obtained by trial-and-error.

In general, the VFC parameters are very much dependent on the system characteristics. The relation between changes in the operating voltage and hence frequency can be derived from (1) and (13) as follows:

$$\Delta f'(t) = -f_0 P_0 \frac{((V+\Delta V)^{n_p} - V^{n_p})}{2HV_0^{n_p}} \tag{17}$$

Assuming that $V_0 = 1$ pu and the system is operating at its nominal voltage prior to any change, (17) can be re-written as:

$$\Delta V = (\Delta f'(t)\mu + 1)^{1/n_p} - 1 \tag{18}$$

where, $\mu = \frac{-2H}{f_0 P_0}$ reflects the system characteristics, since the inertia constant H, nominal frequency f_0, power P_0, and voltage index n_p determine the voltage frequency dependency.

C. Impact of the VFC on Small-Perturbation Stability

Small-perturbation analysis is carried out using eigenvalue studies with the system linearized around a nominal operating point [24]. However, this approach is limited to systems in balanced conditions, which is not the case in general for microgrids [28]. Hence, this paper utilizes a modal estimation approach, in particular the Prony technique, to estimate the system eigenvalues [29]. Thus, the generator speed signal $\omega(t)$ is extracted in continuous form and sampled in discrete form $\omega(k)$, and is represented as a sum of n damped complex sinusoids, as follows:

$$\omega(t) = \sum_{i=1}^{n} \bar{R}_i e^{\lambda_i t} = \sum_{i=1}^{n/2} A_i e^{\alpha_i t} cos\left(\beta_i t + \Phi_i\right) \tag{19}$$

$$\omega(k) = \sum_{i=1}^{n} \bar{R}_i Z_i = \sum_{i=1}^{n} \bar{R}_i e^{\lambda_i T_s} \tag{20}$$

where $\bar{R}_i$ is an output residue corresponding to the mode $\lambda_i = \alpha_i + j\beta_i$, T_s is the sampling time, $A_i = 2|\bar{R}_i|$, and k is the discrete time. According to the Prony method, λ_i and $|\bar{R}_i|$ can be calculated considering that (20) is the solution to a difference equation with order n:

$$\omega(k) = -a_1\omega(k-1) - a_2\omega(k-2) - \cdots - a_n\omega(k-n) \tag{21}$$

this model is often referred to as an auto-regressive model [30], where the output is dependent on the past outputs.

Re-writing (21) in a matrix form results in the following:

$$\Omega = D\theta \tag{22}$$

$$\Omega = [\omega_{k+n}\ \omega_{k+n+1}\ \omega_{k+n+2}\ \ldots\ \omega_{k+N}]^T_{N-n+1} \tag{23}$$

$$\theta = [-a_1\ -a_2\ \ldots\ -a_n]^T \tag{24}$$

$$D = \begin{bmatrix} \omega_{k+n-1} & \omega_{k+n-2} & \cdots & \omega_k \\ \omega_{k+n} & \omega_{k+n-1} & \cdots & \omega_{K+1} \\ \vdots & & & \\ \omega_{k+N-1} & \omega_{k+N-2} & \ldots & \omega_{k+N-n} \end{bmatrix} \tag{25}$$

where N is the number of samples. A least square method can be utilized to compute θ, and the system characteristic equation can be formed using the vector θ as follows:

$$Z^n + a_1 Z^{n-1} + a_2 Z^{n-2} + \cdots + a_n = 0 \tag{26}$$

The eigenvalues of the system are the roots of (26). In this study, the number of complex sinusoids, i.e. the number of the complex poles of the system is considered to be 8; This number is chosen by trial and error, with 8 modes giving the closest estimation of the input signal. The calculations are carried out here using the MATLAB built-in Prony function, as discussed in Section IV.

IV. Case Studies and Simulation Results

To demonstrate the effectiveness of the proposed VFC, a test system, based on the Cigre benchmark for medium voltage distribution network [31] is implemented in PSCAD/EMTDC, with two diesel-based synchronous machines along with three DERs. The general schematic of the test system is shown in Fig. 4. The total load of the system is about 7 MVA, distributed among the buses so as to have an unbalanced load. Feeders are modelled as coupled π sections.

The DERs are connected through bi-directional VSCs that are fully modelled as shown in Fig. 2, including PWM schemes, $abd \leftrightarrow dq$ blocks, PLLSs, and control blocks. These are modelled as ideal dc sources, and their active power output is modelled using actual measurements from an actual low-voltage 300 kW wind turbine, measured over 185s with a resolution of 0.1s (Fig. 5). For the purpose of this study, DER#1 comprises five sub-units, DER#2 two sub-units, and DER#3 4 sub-units, with each sub-unit output the same as the power depicted in Fig. 5; hence, the nominal ratings of the DERs are 1.5 MW, 600 kW and 1.2 MW respectively.

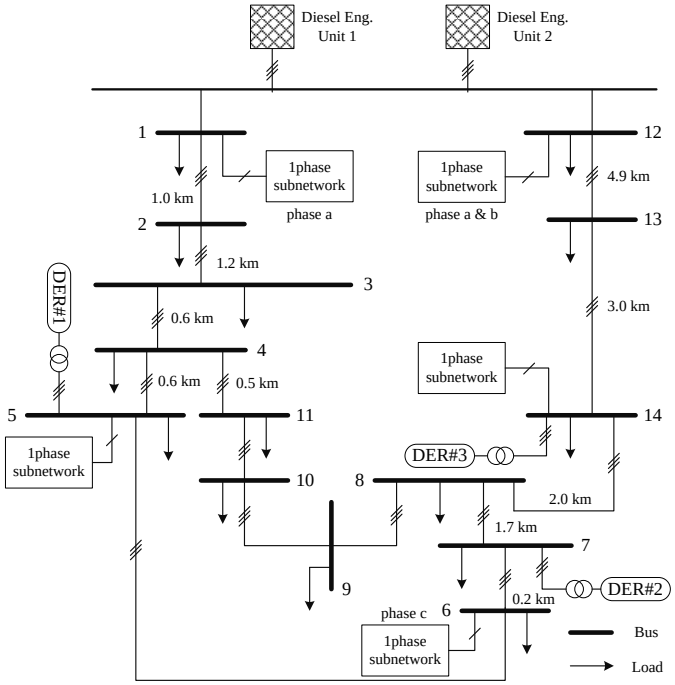

Fig. 4. Test microgrid based on a medium voltage distribution network benchmark [31].

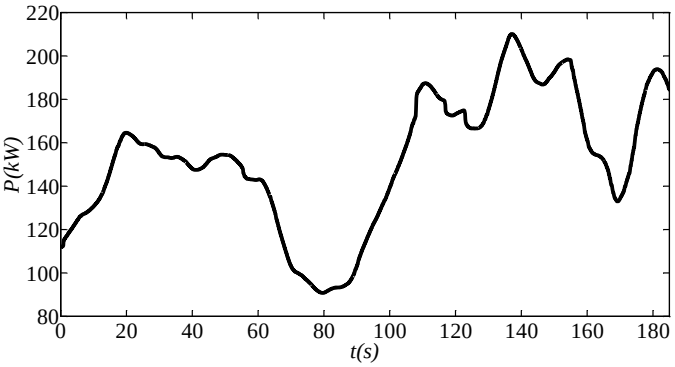

Fig. 5. Low-voltage 300 kW wind turbine measured power output.

The synchronous machines nominal rating is 5.4 MVA combined. In most of the cases discussed here, the two synchronous machines are in charge of regulating the voltage, and the DERs are operating under the CCM paradigm with unity power factor and no contribution to voltage regulation, since in isolated microgrids, the voltage is dominantly controlled by the synchronous machine voltage regulation systems, the VFC is implanted on the exciters of these machines. Thus, the synchronous machines correspond to master controls regulating the voltage and frequency, and the DERs are the slave controls supplying active power to the system. The standard IEEE AC1A excitation systems are used in this work [32]. The parameters of the VFC are tuned by trail-and-error to obtain an acceptable performance, and are given in Table I. It should be mentioned that two lead-lag filters have been used to obtain the best performance of the controller; hence, in Table I, τ_1 and τ_2 are the parameters of the first filter and τ_1' and τ_2' are the parameters of the second filter.

TABLE I
VFC PARAMETERS

Parameter	Value	Parameter	Value	Parameter	Value
K_P	0.2	τ_i	2.65	τ_1	0.01
τ_2	0.9	τ_1'	0.01	τ_2'	0.25

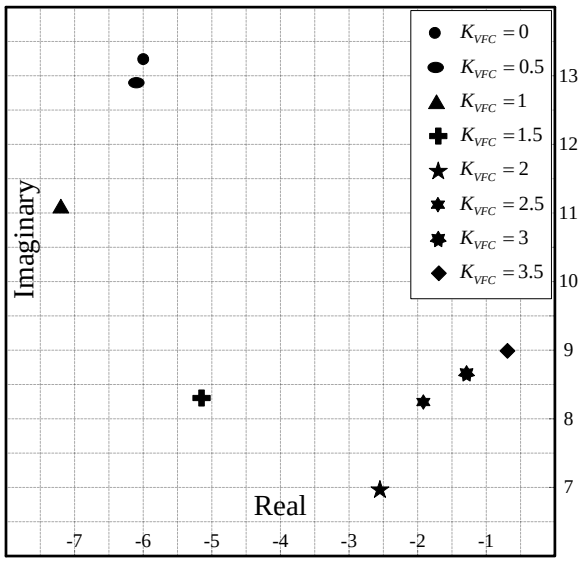

Fig. 6. Dominant eigenvalue for different values of K_{VFC}.

TABLE II
CRITICAL EIGENVALUE DAMPING

K_{VFC}	ζ	K_{VFC}	ζ
0	0.422	0.5	0.432
1	0.539	1.5	0.532
2	0.307	2.5	0.229
3	0.148	3.5	0.076

A. Dominant Eigenvalues vs. K_{VFC}

Dominant eigenvalues are monitored to evaluate the impact of the VFC on the system small-perturbation stability. Figure 6 shows the trajectories of the critical eigenvalue with respect to changes in K_{VFC}, from 0 (VFC not in effect) to 3.5; this eigenvalue corresponds to the low-frequency dominant mode of the system, and is largely sensitive to the controlling parameters. From Fig. 6, it can be seen that as K_{VFC} increases, it reaches a point that for further increase of the gain the system overall damping deteriorate. Table II summarizes the critical eigenvalue damping with respect to changes in K_{VFC}. Observe that $K_{VFC} = 1$ yields the best result, and hence is adopted here as the VFC gain for the test microgrid.

B. VFC vs. Fast-Acting ESS (Scenario 1)

The effectiveness of the VFC during wind fluctuations is demonstrated by comparing the response of the system with and without the VFC. The initial wind generation penetration level of the system is around 20%, and increases up to 40% as per Fig. 5.

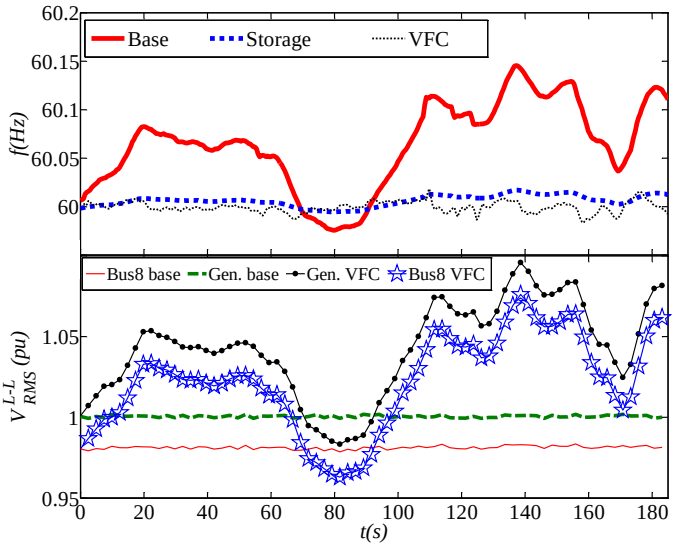

Fig. 7. Voltage and frequency response of the system due to wind fluctuations (Scenario 1).

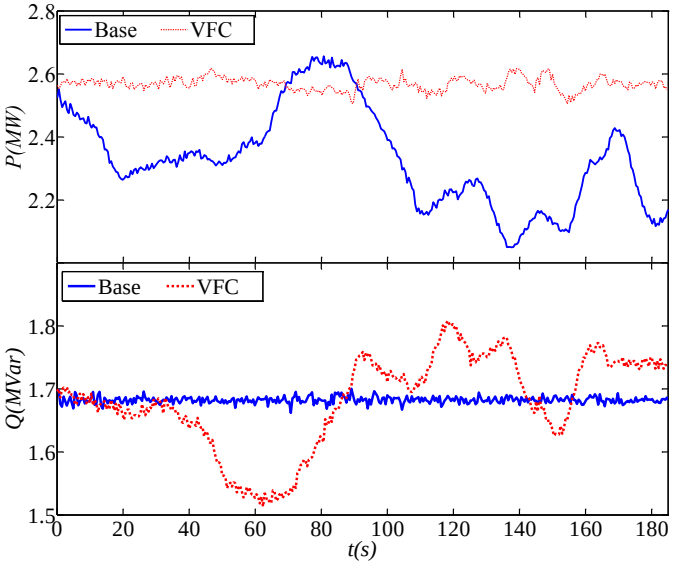

Fig. 8. Active and reactive power injection of diesel Unit 1 with and without the VFC (Scenario 1).

Figure 7 presents the frequency response of the base system without (solid line) and with the proposed VFC (dotted line), and the RMS three-phase line-to-line voltages for the generator bus and Bus 8. The active and reactive power generation of diesel Unit 1 is shown in Fig. 8, with diesel Unit 2 exhibiting the same power injections. Note that the VFC is capable of providing a smooth frequency response as wind output fluctuates, even for a significant penetration of up to 40% of the total power in the system. This is especially significant, since the system with the VFC has no storage. Observe that the voltage variations are kept within the operating voltage range of 0.88-1.1 pu, which is acceptable in isolated microgrids [33]. Also, observe that the active power output of the diesel generators with the VFC has no significant change since the VFC compensates for the wind variations.

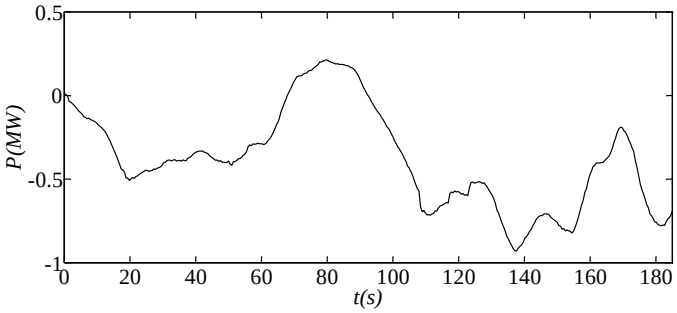

Fig. 9. Active power output of the ESS due to wind fluctuations (Scenario 1).

To better evaluate the effectiveness of the VFC, the frequency response of the system with a fast-acting ESS and no VFC is also shown in Fig. 7. The fast-acting ESS control strategy is similar to the one discussed in [22], and its battery is modelled based on the battery model proposed in [34]. This ESS is connected to Bus 9, and operates at unity power factor under the CCM paradigm; it is charged or discharged according to the power imbalance in the system and has a regulating capacity of 30 MW/Hz, which is a high power-frequency droop, considering that normal ESS droops are in the range of 1 MW/Hz. Such a high droop is chosen for the ESS to achieve a frequency response similar to that of the VFC. Observe from the plot of the output active power of the ESS (Fig. 9), that the ESS absorbs up to 1 MW of active power and about 20 kWh of energy is exchanged with the microgrid. Assuming that the initial state of charge (SOC) of the battery is 20%, the minimum capacity of storage required for this scenario over the course of 180 seconds is almost 25 kWh. Assuming that wind fluctuations will follow the same pattern for an hour, thus the ESS should be as large as 0.5 MWh. Hence, since valve regulated lead-acid (VRLA) batteries are among the most common batteries used in isolated microgrids, such an ESS would be quite expensive, as the procurement price for the VRLA ranges from $5 million to up to $12 million per MWh [35], without considering the price of operation and maintenance. Thus, the implementation of the proposed VFC can bring significant savings by reducing the need for ESS.

C. Disconnection of DER Units (Scenario 2)

To demonstrate the effectiveness of the proposed VFC during large disturbances, all the DERs are disconnected at $t = 1$s. Prior to disconnection, the microgrid is assumed to be in steady-state, and the instantaneous wind power penetration is about 30%, i.e. the DERs are generating more than 2 MW of active power. Figure 10 demonstrates the frequency response and the RMS three-phase line-to-line voltage of the generator bus for the base system (solid line) and for the proposed VFC (dashed line). Also, the active and reactive power injection of diesel Unit 1 is illustrated in Fig. 11, with diesel Unit 2 exhibiting the same power injection. Observe that for the base system, the frequency drops below 59.8 Hz after the disturbance, which is considered as the minimum acceptable operating frequency of microgrids by some utilities

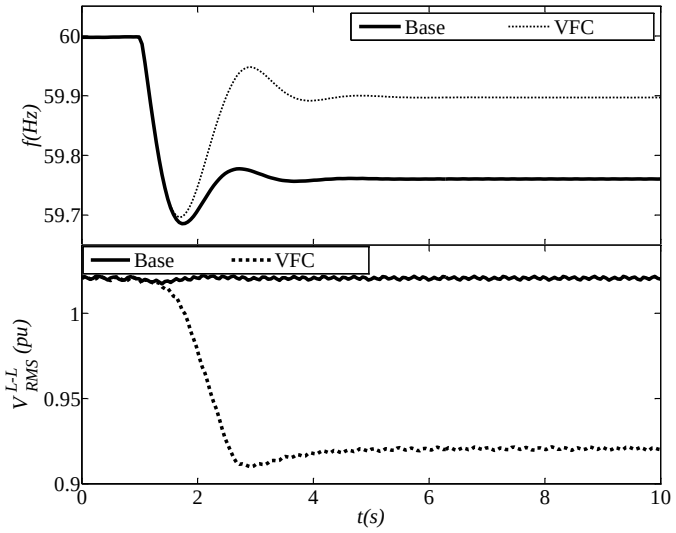

Fig. 10. Voltage and frequency response of the system before, during, and after the disconnection of DER units (Scenario 2).

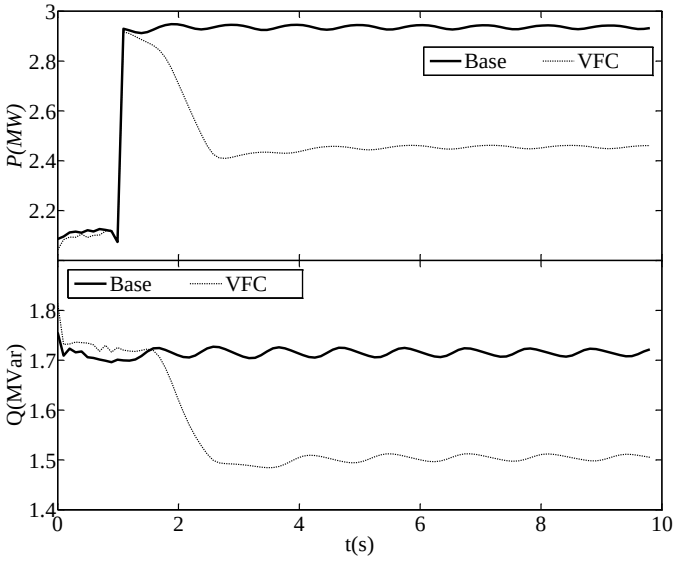

Fig. 11. Active and reactive power injection of diesel Unit 1 with and without the VFC (Scenario 2).

[33]; therefore, the base system would require load shedding for appropriate operation. On the other hand, the frequency response of the system with the VFC is significantly improved with a steady-state frequency around 59.9 Hz, while the voltage remains within acceptable limits according to [33]; hence, the system does not require load curtailment.

Note that the lower voltage limit for the VFC operation is set to 0.92 pu, which is 0.04 pu higher than the minimum permitted operating voltage, so that the voltage drops through the feeders as the distance increases from the generator bus, do not exceed the maximum allowed values in steady-state. For a typical-size isolated microgrid, voltage drops through the feeders would be around 1-2 percent, as shown by the voltages at Bus 5, Bus 8, Bus 7, and Bus 14 depicted in Fig. 12; observe that all these voltages remain within the acceptable range of operation, with a voltage drop of no more than 0.02 pu with

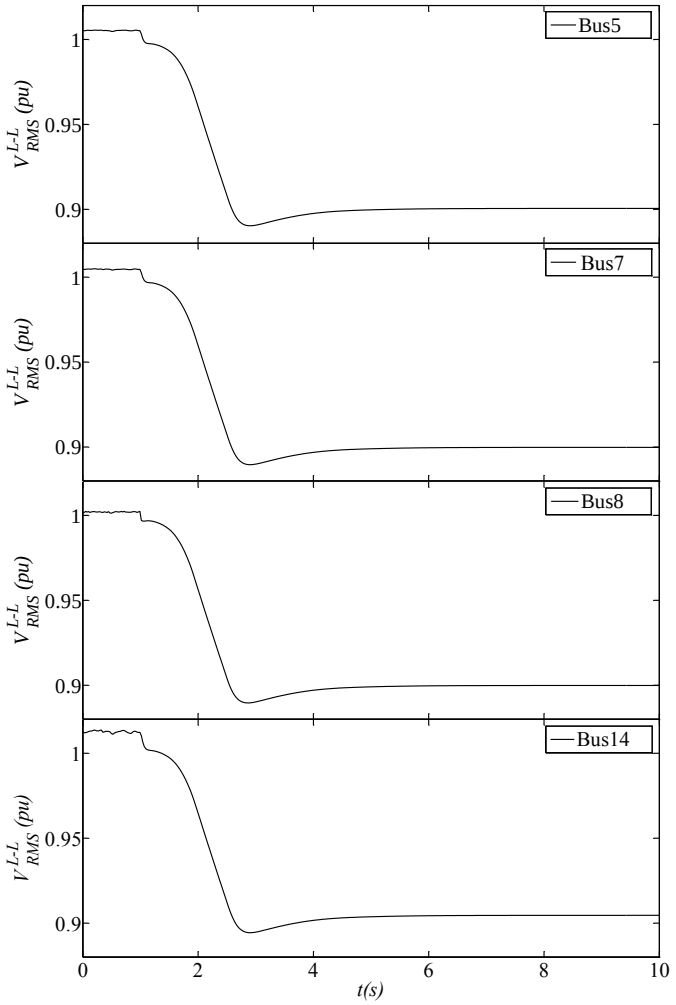

Fig. 12. Voltages at different buses of the system (Scenario 2).

respect to the Gen. Bus.

D. Effect of Operating Voltage Limit (Scenario 3)

In all previous cases, the voltage limit is considered to be 0.92-1.1 pu at the generation bus. Hence, to show the impact of these limits on the VFC performance, new voltage limits of 0.95-1.05 pu are used instead. Figure 13 shows a comparison of the frequency responses and the RMS line-to-line voltage of the generation bus for the different voltage limits. Note that the frequency response is the same when the voltage is within ± 0.05 pu of the nominal voltage, i.e. before $t = 110$ s. However, once the voltage reaches a 1.05 pu limit, the VFC is not capable of regulating the frequency anymore, since decreasing the operating voltage limit decreases the virtual reserve that the VFC can provide to the system, and thus reduces its frequency regulation capability.

E. Effect of Load Modelling (Scenario 4)

As discussed in Section III, the performance of the VFC directly depends on n_p, thus to see its impact on the proposed VFC mechanism n_p is set to 1.2. Figure 14 shows a comparison of the frequency responses, for both values of n_p. Observe

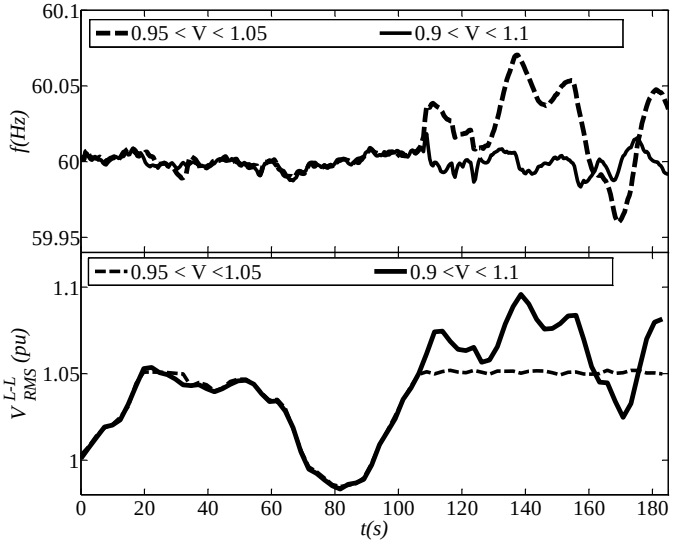

Fig. 13. Voltage and frequency response of the system with different voltage limits (Scenario 3).

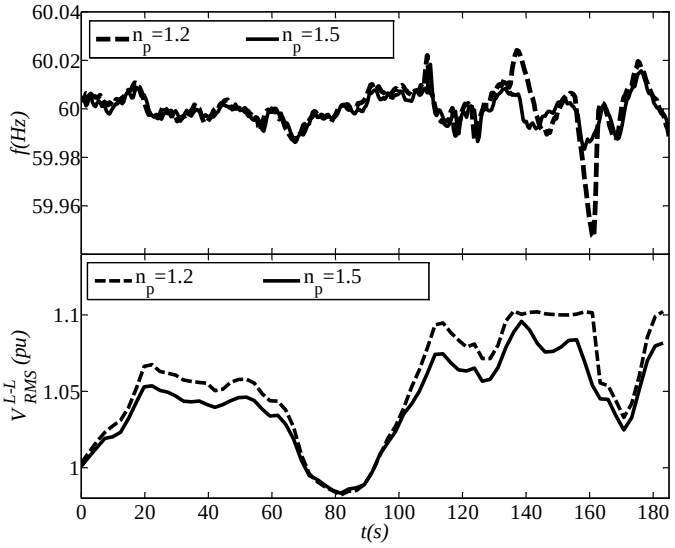

Fig. 14. Voltage and frequency response of the system with different n_p (Scenario 4).

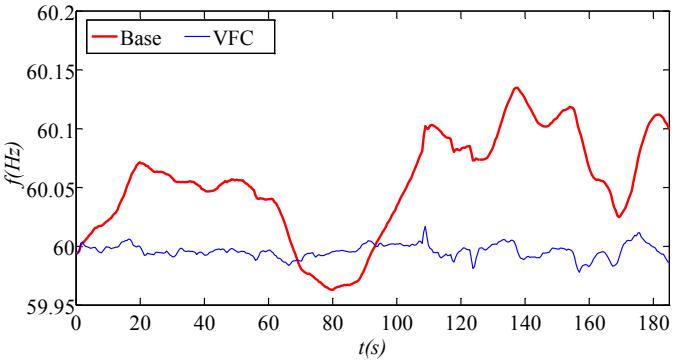

Fig. 15. Frequency response of the system with and without the VFC (scenario 5).

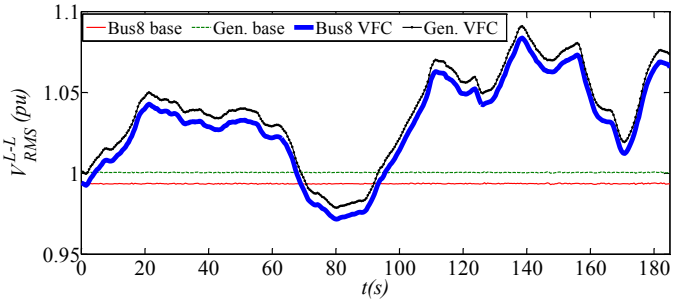

Fig. 16. Voltage response of the system with with and without the VFC (scenario 5).

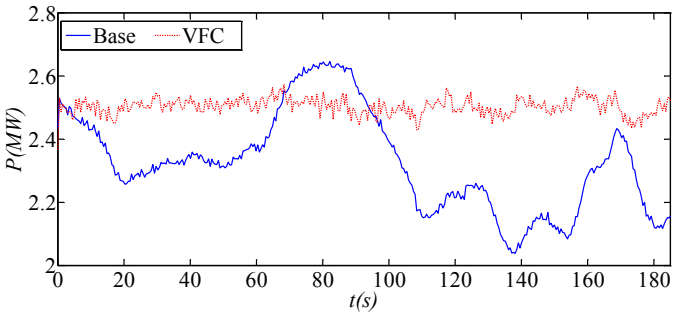

Fig. 17. Active power injection of diesel Unit 1 with and without the VFC (scenario 5).

that as the voltage-dependency of the loads decreases, i.e. as n_p decreases, the voltage variations increase and thus reach a limit between $t = 120$ s to $t = 160$ s, as expected. However, the VFC still manages to properly regulate the effect of the wind fluctuations on the system frequency.

F. Diesel Units at Different Buses (Scenario 5)

In all previous cases, both diesel generators are connected at the Gen. Bus. Hence, in the test discussed next, the diesel Unit 2 is connected at Bus 5, while the diesel Unit 1 remains connected at the Gen. Bus; both generator ratings and parameters are the same as before. The same test scenario as the one in Section IV-B is then carried out, where the effectiveness of the VFC during wind fluctuations is demonstrated by comparing the response of the system with and without the VFC.

Figure 15 demonstrates the frequency response of the system with and without the VFC. Voltages at the Gen. Bus and Bus 8 are shown in Fig. 16; the active power output of Unit 1 is shown in Fig. 17 with Unit 2 exhibiting the same active power response. The reactive output of both units are shown in Fig. 18 and Fig. 19, respectively. Observe in Figs. 15-19 that the system shows similar satisfactory performance as in the previous cases, with the frequency close to 60 Hz and the voltages within acceptable operating limits.

G. Discussion

There are some aspects of the system that should be carefully taken into consideration. First, as shown in (13), the performance of the VFC depends on the system load composition; this can also be concluded by comparing the results presented in Sections IV-A and IV-E. Hence, in systems

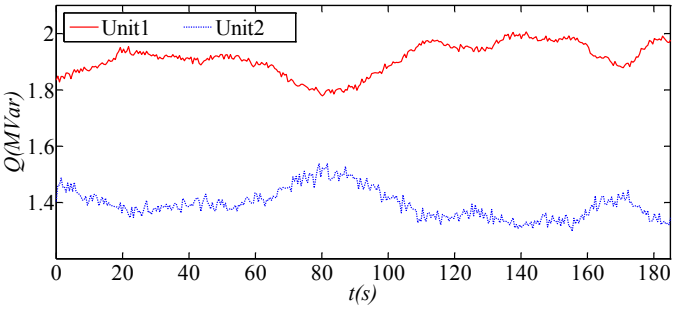

Fig. 18. Reactive power injection of diesel Unit 1 and Unit 2 without the VFC (scenario 5).

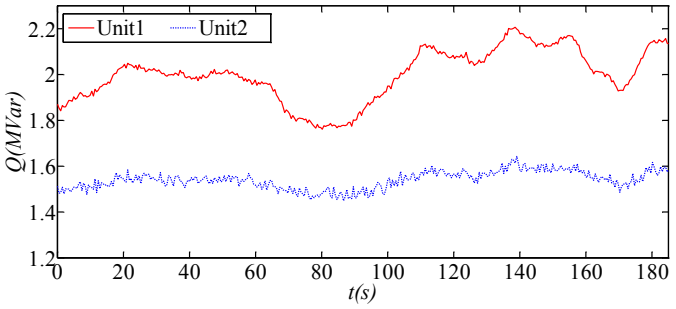

Fig. 19. Reactive power injection of diesel Unit 1 and Unit 2 with the VFC (scenario 5).

with very low voltage index n_P, the VFC would not be able to regulate the frequency. However, the focus of this paper is on isolated microgrids, such as those that exist in remote communities, where loads are dominantly residential, with n_P often higher than 1.1% [36]–[39]. For these types of microgrids, experimental results are provided in [40] demonstrating the viability of frequency regulation through load voltage control; thus, for the archipelago of Guadeloupe in France, a 2.4% change in the voltage results in 3.5% change in the actual power consumption. According to (13), this implies that the voltage index for such a system could be $n_P = 1.47$, which is in the range used in this paper. The authors also show that a 5% change in the voltage reference set-point of the generators will significantly improve the system transient frequency response for an 8% generation loss disturbance.

Second, the grid size will affect the VFC performance as well. Thus, for very large systems, changing the generators output voltage will not necessarily decrease remote bus voltages. Additionally, for systems with long inductive feeders, the voltage drop for end-feeders may be significant, thus limiting the operating range of the VFC. However, both scenarios are unlikely to be an issue for isolated microgrids, where the size of the grid is typically in the order of a few km. Observe that the test system used in this paper is relatively large, with feeders as long as 5 km and buses as far as 10 km from the Gen. Bus. However, the results show that the VFC is capable of regulating the frequency, while all the voltages in the system remain within acceptable operating ranges.

V. Conclusion

A fast voltage-based frequency controller has been proposed in this paper for isolated/islanded microgrids, acting as an additional control to conventional frequency controllers to improve frequency response of the system. Based on realistic analysis and results presented in this paper, the proposed controller is simple, has a straightforward implementation, and is easily applicable to a variety of different systems and voltage regulation devices (e.g. synchronous machines, DERs with voltage regulation capacity).

The proposed controller offers several advantages, reducing the dependency of a microgrid with high renewable energy sources penetration on ESS, which makes these types of microgrids more viable. Hence, the VFC can play the role of a virtual storage, with capacity depending on the operating voltage levels and type of loads. In addition, the controller can be very effective in minimizing the impact of large disturbances on the system such as loss of a generation, enhancing small-perturbation stability by providing more damping for the system. The controller also provides zero steady-state error with respect to existing frequency control techniques, and requires no additional investment or communication infrastructure. Finally, its response is almost instantaneous, and since the voltage can be kept within acceptable limits, it has no significant impact on customer quality of service. However, its performance is dependent on the load mix and overall voltage ranges.

References

[1] N. Hatziargyriou, H. Asano, R. Iravani, and C. Marnay, "Microgrids," *IEEE Power Energy Mag.*, vol. 5, no. 4, pp. 78–94, July 2007.

[2] *IEEE Guide for Design, Operation, and Integration of Distributed Resource Island Systems with Electric Power Systems*, IEEE Std. 1547.4, 2011.

[3] J. M. Guerrero, F. Blaabjerg, T. Zhelev, K. Hemmes, E. Monmasson, S. Jemei, M. P. Comech, R. Granadino, and J. I. Frau, "Distributed generation: toward a new energy paradigm," *IEEE Ind. Electron. Mag.*, pp. 52–64, March 2010.

[4] G. Delille, B. Franois, and G. Malarange, "Dynamic frequency control support by energy storage to reduce the impact of wind and solar generation on isolated power system's inertia," *IEEE Trans. Sustain. Energy*, vol. 3, no. 4, pp. 931–939, Nov. 2012.

[5] C. Yuen, A. Oudalov, and A. Timbus, "The Provision of Frequency Control Reserves From Multiple Microgrids," *IEEE Trans. Ind. Electron.*, vol. 58, no. 1, pp. 173–183, Jan. 2011.

[6] J. M. Guerrero, M. Chandorka, T. Lee, and P. C. Loh, "Advanced Control Architectures for Intelligent Microgrids–Part I: Decentralized and Hierarchical Control," *IEEE Trans. Ind. Electron.*, vol. 60, no. 4, pp. 1254–1262, April 2012.

[7] J. M. Guerrero, P. C. Loh, T. Lee, and M. Chandorkar, "Advanced Control Architectures for Intelligent Microgrids–Part II: Power Quality, Energy Storage, and AC/DC Microgrids," *IEEE Trans. Ind. Electron.*, vol. 60, no. 4, pp. 1263–1270, April 2012.

[8] D. E. Olivares, A. Mehrizi-Sani, A. H. Etemadi, C. A. Cañizares, R. Iravani, M. Kazerani, A. H. Hajimiragha, O. Gomis-Bellmunt, M. Saeedifard, R. Palma-Behnke *et al.*, "Trends in Microgrid Control," *IEEE Trans. Smart Grid*, vol. 5, no. 4, pp. 1905–1919, May 2014.

[9] M. C. Chandorkar, D. M. Divan, and R. Adapa, "Control of parallel connected inverters in standalone ac supply systems," *IEEE Trans. Ind. Appl.*, vol. 29, no. 1, pp. 136–143, Jan. 1993.

[10] N. Pogaku, M. Prodanovic, and T. C. Green, "Modeling, analysis and testing of autonomous operation of an inverter-based microgrid," *IEEE Trans. Power Electron.*, vol. 22, no. 2, pp. 613–625, March 2007.

[11] Y. A.-R. I. Mohamed and E. F. El-Saadany, "Adaptive Decentralized Droop Controller to Preserve Power Sharing Stability of Paralleled Inverters in Distributed Generation Microgrids," *IEEE Trans. Power Electron.*, vol. 23, no. 6, pp. 2806–2816, Nov. 2008.

[12] J. Kim, J. M. Guerrero, P. Rodriguez, R. Teodorescu, and K. Nam, "Mode Adaptive Droop Control With Virtual Output Impedances for an Inverter-Based Flexible AC Microgrid," *IEEE Trans. Power Electron.*, vol. 26, no. 3, pp. 689–701, Nov. 2010.
[13] R. Majumder, B. Chaudhuri, A. Ghosh, G. Ledwich, and F. Zare, "Improvement of Stability and Load Sharing in an Autonomous Microgrid Using Supplementary Droop Control Loop," *IEEE Trans. Power Syst.*, vol. 25, no. 2, pp. 796–808, Oct. 2009.
[14] R. Majumder, G. Ledwich, A. Ghosh, S. Chakrabarti, and F. Zare, "Droop Control of Converter-Interfaced Microsources in Rural Distributed Generation," *IEEE Trans. Power Del.*, vol. 25, no. 4, pp. 2768–2778, March 2010.
[15] R. Majumder, A. Ghosh, G. Ledwich, and F. Zare, "Load sharing and power quality enhanced operation of a distributed microgrid," *IET Renew. Power Gener.*, vol. 3, no. 2, pp. 109–119, June 2009.
[16] M. Arriaga, C. Cañizares, and M. Kazerani, "Northern Lights: Access to Electricity in Canada's Northern and Remote Communities," *IEEE Power Energy Mag.*, vol. 12, no. 4, pp. 50–59, August 2014.
[17] G. Lalor, A. Mullane, and M. O'Malley, "Frequency control and wind turbine technologies," *IEEE Trans. Power Syst.*, vol. 20, no. 4, pp. 1905–1913, Nov. 2005.
[18] F. C. Schweppe, R. D. Tabors, J. L. Kirtley, H. R. Outhred, F. H. Pickel, and A. J. Cox, "Homeostatic utility control," *IEEE Trans. Power App. Syst.*, vol. 99, no. 3, pp. 1151–1163, May 1980.
[19] D. J. Hammerstrom, J. Brous, D. P. Chassin, G. R. Horst, R. Kajfasz, P. . Michie, T. Oliver, T. A. Carlon, C. Eustis, O. M. Jervegren *et al.*, "Part II. Grid Friendly™ appliance Project," Pacific Northwest National Laboratory, Richland, Washington, Tech. Rep. PNNL-17079, Oct. 2007.
[20] A. Molina-Garcia, F. Bouffard, and D. Kirschen, "Decentralized Demand-Side Contribution to Primary Frequency Control," *IEEE Trans. Power Syst.*, vol. 26, no. 1, pp. 411–419, May 2010.
[21] M. Kayikçi and J. Milanović, "Dynamic contribution of DFIG-based wind plants to system frequency disturbances," *IEEE Trans. Power Syst.*, vol. 24, no. 2, pp. 859–867, May 2009.
[22] G. Dellile, B. Francois, and G. Malarange, "Dynamic Frequency Control Support by Energy Storage to Reduce the Impact of Wind and Solar Generation on Isolated Power System's Inertia," *IEEE Trans. Sustain. Energy*, vol. 3, no. 4, pp. 931–939, Oct. 2012.
[23] J. Bomer, K. Burges, C. Nabe, and M. Poller, "All island TSO facilitation of renewables study - Final report for work package 3," EirGrid, Ecofys, Germany, Tech. Rep. PEGEDE083532, June 2010.
[24] P. Kundur, *Power System Stability and Control*. New York, US: McGraw-hill Professional, 1994.
[25] IEEE Committee Report, "Computer representation of excitation systems," *IEEE Trans. Power App. Syst.*, vol. 87, no. 6, pp. 1460–1464, June 1968.
[26] J. D. Glover, M. Sarma, and T. Overbye, *Power System Analysis & Design*. Stamford, US: Cengage Learning, 2011.
[27] A. J. Collin, G. Tsagarakis, A. E. Kiprakis, and S. McLaughlin, "Development of Low-Voltage Load Models for the Residential Load Sector," *IEEE Trans. Power Syst.*, vol. 29, no. 5, pp. 2180–2188, Feb. 2014.
[28] E. Nasr-Azadani, C. A. Canizares, D. E. Olivares, and K. Bhattacharya, "Stability Analysis of Unbalanced Distribution Systems With Synchronous Machine and DFIG Based Distributed Generators," *IEEE Trans. Smart Grid*, vol. 5, no. 5, pp. 2326–2338, Sep. 2014.
[29] H. Ghasemi, "On-Line Monitoring and Oscillatory Stability Margin Prediction in Power Systems Based on System Identification," Ph.D. dissertation, Univ. of Waterloo, Waterloo, ON, Aug. 2006.
[30] J. R. Smith, F. Fatehi, C. S. Woods, J. F. Hauer, and D. J. Trudnowski, "Transfer function identification in power system applications," *IEEE Trans. Power Syst.*, vol. 8, no. 3, pp. 1282–1290, Aug. 1993.
[31] K. Strunz, "Developing benchmark models for studying the integration of distributed energy resources," in *Proc. IEEE Power Eng. Soc. Gen. Meeting*, Montreal, QC, July 2006.
[32] *IEEE Recommended Practice for Excitation System Models for Power System Stability Studies*, IEEE Std. 421.5, 1992.
[33] "Distributed Generation Technical Interconnection Requirements: Interconnections at Voltages 50kV and Below," Hydro One Networks INC., Toronto, Ontario, Tech. Rep. DT-10-015 R3, Mar. 2013.
[34] O. Tramblay, L. A. Dessaint, and A. I. Dekkiche, "A Generic Battery Model for the Dynamic Simulation of Hybrid Electric Vehicles," in *Proc. IEEE Vehicle Power and Propulsion Conf.*, Arlington, TX, Sep. 2007.
[35] A. A. Akhil, G. Huff, A. B. Currier, B. C. Kaun, D. M. Rastler, S. B. Chen, A. L. Cotter, D. T. Bradshaw, and W. D. Gauntlett, "DOE/EPRI 2013 Electricity Storage Handbook in Collaboration with NRECA," Sandia National Laboratories, Livermore, California, Tech. Rep. SAND2013-5131, July 2013.
[36] Z. Wang and J. Wang, "Review on implementation and assessment of conservation voltage reduction," *IEEE Trans. Power Syst.*, vol. 29, no. 3, pp. 1306–1315, May 2014.
[37] J. C. Erickson and S. R. Gilligan, "The effects of voltage reduction on distribution circuit loads," *IEEE Trans. Power App. Syst.*, vol. 101, no. 7, pp. 2014–2018, July 1982.
[38] V. J. Warnock and T. L. Kirkpatrick, "Impact of voltage reduction on energy and demand: Phase ii," *IEEE Trans. Power Syst.*, vol. 1, no. 2, pp. 92–95, May 1986.
[39] Z. Wang, M. Begovic, and J. Wang, "Analysis of conservation voltage reduction effects based on multistage svr and stochastic process," *IEEE Trans. Smart Grid*, vol. 5, no. 1, pp. 431–439, Jan. 2014.
[40] G. Delille, L. Capely, D. Souque, and C. Ferrouillat, "Experimental validation of a novel approach to stabilize power system frequency by taking advantage of load voltage sensitivity," in *Proc. of IEEE PowerTech Eindhoven*, June 2015.

Mostafa Farrokhabadi (S'12) received the B.Sc. degree in electrical engineering from Amirkabir University of Technology, Tehran, Iran, in 2010, and the M.Sc. degree in Electric Power Engineering from KTH Royal Institute of Technology, Stockholm, Sweden, in 2012. He is currently a Ph.D. candidate in the Electrical and Computer Engineering Department at the University of Waterloo, ON, Canada. His research interests includes modeling, control, and optimization in microgrids.

Claudio A. Cañizares (S85, M91, SM00, F07) received in April 1984 the Electrical Engineer Diploma from the Escuela Politécnica Nacional (EPN), Quito-Ecuador, where he held different teaching and administrative positions from 1983 to 1993. His MS (1988) and PhD (1991) degrees in Electrical Engineering are from the University of Wisconsin-Madison. Dr. Cañizares has held various academic and administrative positions at the E&CE Department of the University of Waterloo since 1993, where he is currently a full Professor, the Hydro One Endowed Chair and the Associate Director of the Waterloo Institute for Sustainable Energy (WISE). His research activities concentrate on the study of modeling, simulation, control, stability, computational and dispatch issues in sustainable power and energy systems in the context of competitive markets and Smart Grids.

Kankar Bhattacharya Kankar Bhattacharya (M95, SM01) received the Ph.D. degree in Electrical Engineering from the Indian Institute of Technology, New Delhi, India in 1993. He was in the faculty of Indira Gandhi Institute of Development Research, Mumbai, India, during 1993-1998, and then the Department of Electric Power Engineering, Chalmers University of Technology, Gothenburg, Sweden, during 1998-2002. He joined the E&CE Department of the University of Waterloo, Canada, in 2003 where he is currently a full Professor. His research interests are in power system economics and operational aspects.